scientific reports

Check for updates

OPEN

Functional extracellular vesicles enable injectable hydrogels with stable osteogenic properties for minimally invasive bone defect repair

Guangliang Liu[1,2,4], Zhengsong Xie[3,4], Xinxing Fu[1] & Mingjun Wu[2]✉

The clinical use of bone morphogenetic protein 2 (BMP2) is limited by supraphysiological dosing requirements, which can cause adverse effects such as heterotopic ossification and radiculitis. To address this, we developed a cell-free delivery system using BMP2-enriched extracellular vesicles (BMP2-EVs) derived from mesenchymal stem cells engineered via adenoviral transduction. The BMP2-EVs were thoroughly characterized and combined with an injectable collagen hydrogel for sustained release. In vitro, BMP2-EVs significantly enhanced osteogenic differentiation and mineralized nodule formation in MSCs, while the hydrogel showed high biocompatibility (>92% cell viability) and prolonged BMP2 retention (61% after 14 days). In a mouse femoral defect model, the BMP2-EVs/hydrogel system effectively promoted bone regeneration following minimally invasive injection. This strategy enables localized and sustained BMP2 delivery, mitigates burst release, reduces side effect risks, and presents a clinically promising approach for bone repair.

Keywords Bone morphogenetic protein 2, Extracellular vesicles, Collagen hydrogel, Bone defect, Minimally invasive repair

Severe trauma, malignant tumors, and infectious diseases cause more than 4 million bone defects worldwide each year, posing major challenges in clinical managemen[1]. Since the U.S. Food and Drug Administration (FDA) approved recombinant human bone morphogenetic protein 2 (rhBMP-2) for clinical use in 2002, the Infuse Bone Graft system—which combines an absorbable collagen sponge with BMP2—has been widely employed in orthopedics for over two decades, with its osteogenic efficacy well established[2]. As a key osteoinductive factor, BMP2 not only promotes the osteogenic differentiation of mesenchymal stem cells (MSCs) but also regulates angiogenesis: it participates in vascular network formation during embryogenesis[3] and enhances neovascularization in adult tissues by upregulating CD31 expression[4].

However, the clinical utility of BMP2 remains constrained by its physicochemical properties: (1) Poor affinity with absorbable collagen sponge: Up to 50% of BMP2 is released explosively within 2 days post-implantation, leading to low retention rates[5,6]. (2) Short in vivo half-life (~ 7 min): BMP2 is rapidly cleared after release[7]. (3) Supra-physiological clinical doses (1.5 mg/mL): These exceed physiological concentrations (18.8–22 pg/mL) by orders of magnitude[8,9], causing complications such as ectopic ossification, radiculitis, and soft tissue edema[10]. These limitations underscore the urgent need for novel delivery systems.

Current research on BMP2 carriers primarily focuses on three material systems: Natural polymers (e.g., type I collagen), which suffer from low loading efficiency and uncontrollable degradation[11]. Inorganic materials (e.g., β-tricalcium phosphate), exhibit poor mechanical compatibility with bone tissue. Synthetic polymers (e.g., poly (lactic-co-glycolic acid), PLGA), which can optimize drug release kinetics via core-shell microsphere designs but lack bioactivity[11,12].

In recent years, extracellular vesicles (EVs), particularly those derived from mesenchymal stem cells (MSCs), have emerged as highly promising drug delivery vehicles owing to their favorable biocompatibility

[1]The Second Affiliated Hospital of Chongqing Medical University, Chongqing, China. [2]Innovation Center of Chongqing Medical University, Chongqing, China. [3]Department of Clinical Medical Laboratory, Third People's Hospital of Chengdu, Clinical Medical College of Southwest Jiaotong University, Chengdu, China. [4]Guangliang Liu and Zhengsong Xie contributed equally to this work. ✉email: 100332@cqmu.edu.cn

and targeting capabilities[13]. MSC-EVs inherit various biological functions from their parental cells, including homing to injury sites, modulating immune responses, and promoting angiogenesis. Moreover, these 30–200 nm vesicles exhibit distinctive advantages as delivery carriers[14,15]: (1) Low immunogenicity: The absence of MHC-II expression helps them evade immune rejection and circumvent ethical concerns associated with cell transplantation; (2) Extended half-life: EVs exhibit significantly longer in vivo retention than free proteins; (3) Excellent biocompatibility: As endogenous nanocarriers, they are naturally processed without eliciting harmful responses; (4) Intrinsic bioactive cargo: They carry functional proteins and nucleic acids from donor cells, enabling direct modulation of recipient cell functions.

By genetically engineering donor cells (e.g., via plasmid, adenoviral, or lentiviral transduction) to express target molecules, researchers can isolate extracellular vesicles enriched with the corresponding proteins from conditioned medium[16,17]. EVs exhibit high affinity for extracellular matrix components such as type I collagen[18], which facilitates sustained release of encapsulated growth factors while protecting them from enzymatic degradation[19]. These dual properties make EVs ideal candidates for controlled growth factor delivery.

Hydrogels—including those based on hyaluronic acid, chitosan, or methacrylated gelatin (GelMA)—have demonstrated great potential in bone repair. However, their fabrication generally relies on chemical crosslinking or polymer modification. For example, hyaluronic acid is often crosslinked using 1-ethyl-3-(3-dimethylaminopropyl)carbodiimide (EDC) to form hydrogels for loading MSC-derived exosomes[20]. Similarly, chitosan or GelMA hydrogels are commonly photocrosslinked via UV irradiation in the presence of photoinitiators to encapsulate MSC exosomes[21–23]. Nevertheless, residual crosslinking agents may cause cytotoxicity and inflammatory responses[24].

In this study, we integrated a clinically friendly collagen hydrogel carrier with BMP2-loaded mesenchymal stem cell-derived exosomes (BMP2-EVs) to develop a safe, efficient, and clinically translatable bone regeneration system. This hydrogel undergoes self-crosslinking triggered by body temperature, eliminating the need for any chemical crosslinking agents, thereby ensuring excellent biosafety and superior adaptability to irregular bone defects. We evaluated the system's ability to promote osteogenic differentiation and mineralization of mesenchymal stem cells through in vitro experiments. Furthermore, in vivo studies assessed the efficacy of the cell-free BMP2-EVs-loaded hydrogel in minimally invasive bone repair.

Results

Extraction and characterization of EVs loaded with BMP2 from mesenchymal stem cells

To obtain functional vesicles for BMP2 delivery, we isolated extracellular vesicles (EVs) from the conditioned medium of genetically engineered mesenchymal stem cells (MSCs) and systematically characterized their basic properties and BMP2 loading. After transfecting MSCs for 24 h with recombinant adenovirus expressing green fluorescent protein (Ad-GFP or GFP-labeled Ad-BMP2), GFP fluorescence images were captured using an inverted fluorescence microscope. The observed green fluorescence indicated successful viral transduction and expression of the GFP reporter gene (Fig. 1A).

Quantitative real-time polymerase chain reaction (qRT-PCR) analysis showed that MSCs infected with Ad-BMP2 exhibited significantly higher *Bmp2* expression levels compared to the Ad-GFP control group, whereas the Noggin (a BMP2 inhibitor) group showed decreased *Bmp2* expression ($p < 0.05$, Fig. 1B).

Following ultracentrifugation, EV deposits were visible as a characteristic pellet at the bottom of the tube (Fig. 1C). Transmission electron microscopy revealed typical cup-shaped, vesicle-like structures (Fig. 1D). Nanoparticle tracking analysis indicated that the majority of EV particles fell within the size range of 30–200 nm (Fig. 1E). Western blot analysis confirmed positive expression of the exosome-related proteins Alix, CD63, and TSG101, and negative expression of GM130 (Fig. 1F), collectively verifying the successful extraction of EVs.

BMP2 loading efficiency was evaluated using two methods: (1) Relative loading amount, assessed by Western blot, showed a stronger BMP2 signal in the BMP2-EVs group compared to the Control-EVs group (Fig. 1F, G); (2) Absolute loading quantity, measured by ELISA, demonstrated a BMP2 concentration of 10.65 ± 1.45 ng/μg in BMP2-EVs. This represented a 3.3-fold increase in loading capacity in the Ad-BMP2 group relative to control EVs (Fig. 1H).

Screening for the optimal concentration of BMP2-EVs in inducing osteogenic differentiation

After successful preparation of BMP2-EVs, we determined the optimal concentration for inducing osteogenic differentiation of MSCs. Uptake of DiI-labeled (red) EVs by MSCs was confirmed using fluorescence microscopy (Fig. 2A).

Alkaline phosphatase (ALP) activity was used as an indicator to evaluate the osteoinductive capacity of EVs at different concentrations. After 7 days of culture, BMP2-EVs enhanced ALP activity in MSCs (Fig. 2B). Biochemical quantification showed that the highest ALP activity was achieved with 30 μg/mL BMP2-EVs (Fig. 2C), which was 2.9-fold higher than that in the Control-EVs group ($p < 0.05$).

It's worth noting that raising BMP2-EVs concentration from 30 μg/mL to 60 μg/mL didn't further significantly boost ALP activity. This likely indicates that at 30 μg/mL, the BMP2 signaling pathway is saturated and receptors are fully engaged, so increasing EVs dose won't bring extra osteogenic effects.

Biocompatibility assessment of collagen hydrogels

To construct a three-dimensional delivery platform suitable for cell survival and growth, we prepared collagen hydrogels at different concentrations and evaluated their degradation behavior and biocompatibility with encapsulated MSCs. This collagen solution is injectable and transforms from a liquid state to a hydrogel at 37 ℃ (Fig. 3A).

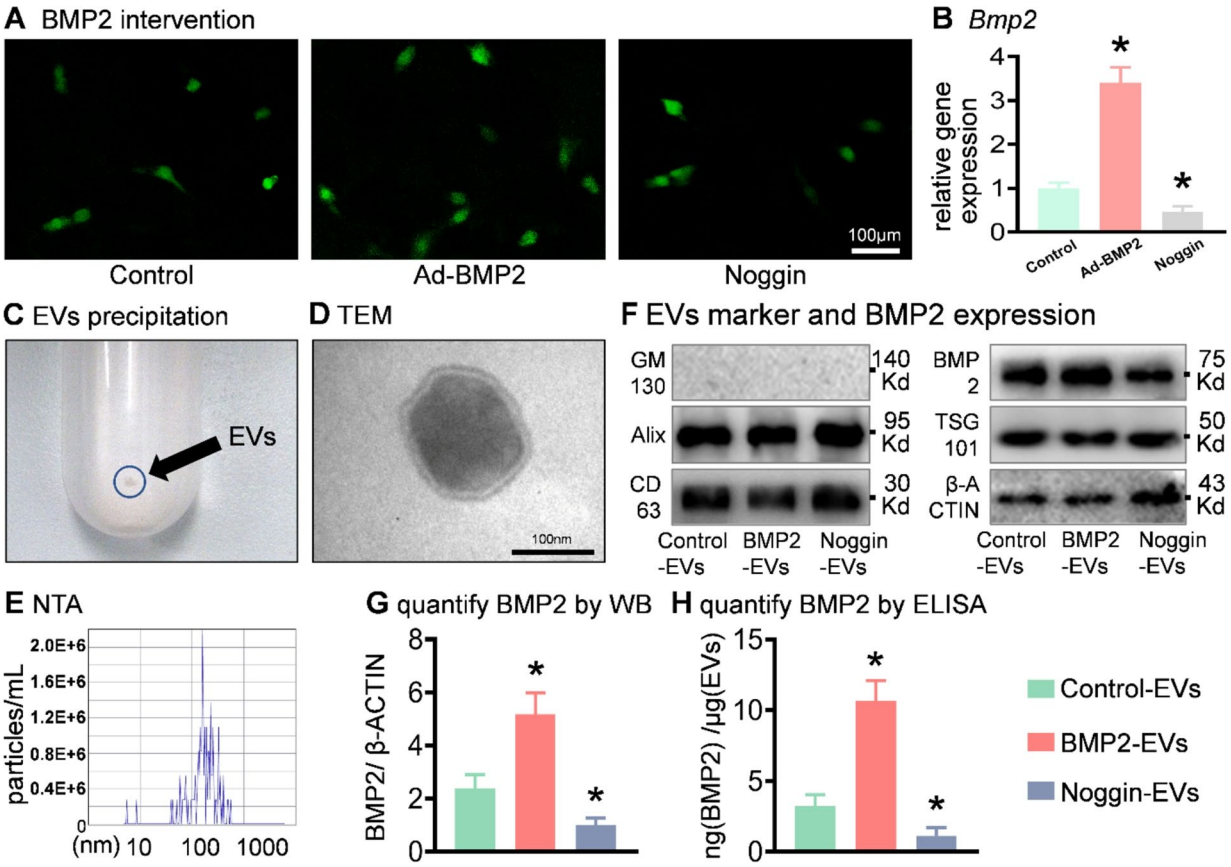

Fig. 1. Extraction and characterization of extracellular vesicles(EVs) loaded with BMP2 from mesenchymal stem cells (MSCs). (A) Experimental groups: (1) Control: MSCs transfected with Ad-GFP adenovirus; (2) Ad-BMP2: MSCs transfected with GFP-labeled-Ad-BMP2 adenovirus to overexpress BMP2; (3) Noggin: MSCs transfected with Ad-GFP adenovirus and treated with Noggin (a BMP2 inhibitor). Green fluorescent protein (GFP) images were captured using an inverted fluorescence microscope. (B) qRT-PCR analysis of Bmp2 gene expression. (C) EV pellet obtained after ultracentrifugation. (D) TEM image of EVs. (E) Nanoparticle tracking analysis (NTA) size distribution profile. (F) Western blot analysis of EV markers. (G) Semi-quantitative analysis of BMP2 by Western blot ($n = 5$). (H) ELISA quantification of BMP2 loading in EVs ($n = 5$). Data are presented as mean ± SD; $^*p < 0.05$ vs. Control group by one-way ANOVA.

The degradation of the hydrogel over a period of 2 weeks was tested under physiological simulation conditions (PBS, pH 7.4, 37 °C). Low-concentration hydrogels (0.5 mg/mL and 1 mg/mL) degraded rapidly, with mass losses of 76% and 43%, respectively, by day 14 (Fig. 3B), indicating insufficient stability for sustained BMP2 release. In contrast, intermediate-to-high concentrations (2 mg/mL and 4 mg/mL) showed significantly slower degradation, with mass losses of 25% and 28% at day 14 ($p > 0.05$), demonstrating comparable stability. Based on degradation performance and material efficiency, the 2 mg/mL concentration was selected for subsequent experiments.

Biocompatibility was assessed using live/dead staining and cell proliferation assays. The BMP2-EVs group maintained cell viability above 92% on days 1, 4, and 7 (Fig. 3C, D). CCK-8 assays indicated good cell proliferation within the hydrogels. BMP2-EVs promoted cell proliferation compared to Control-EVs, whereas the Noggin-EVs group showed reduced proliferative capacity (Fig. 3E).

BMP2-EVs promote osteogenesis and mineralization of MSCs in hydrogels

We next assessed the combined effects of the optimized BMP2-EVs and collagen hydrogel system on osteogenic differentiation and mineralization of MSCs in three-dimensional culture.

Uptake of DiI-labeled EVs by MSCs within the collagen hydrogel was confirmed (Fig. 4A). Osteogenic differentiation levels were assessed using alkaline phosphatase staining, biochemical quantification of alkaline phosphatase activity, and qRT-PCR detection of osteogenic markers. On day 7, the BMP2-EVs group showed more intense ALP staining compared to the Control-EVs group, whereas the Noggin-EVs group exhibited lighter staining (Fig. 4B). ALP activity in the BMP2-EVs and Noggin-EVs groups was 3.6-fold and 0.5-fold that of the Control-EVs group, respectively ($p < 0.05$) (Fig. 4C). qRT-PCR revealed upregulation of osteogenic genes (*Alpl*, *Runx2*, *Col1a1*) in the BMP2-EVs group, while their expression was decreased in the Noggin-EVs

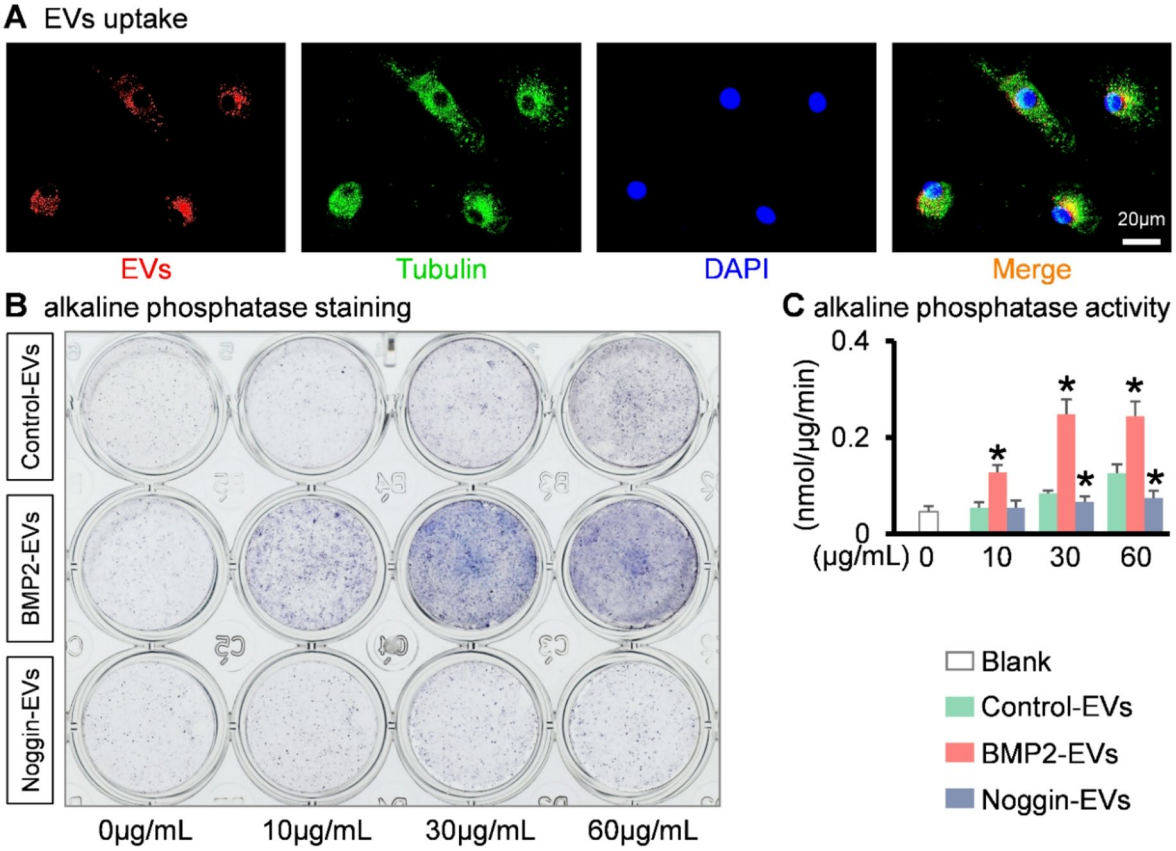

Fig. 2. Optimization of BMP2-EVs concentration for promoting osteogenic differentiation of MSCs. (A) Uptake of red fluorescent-labeled BMP2-EVs by MSCs. MSCs were stained with Tubulin-Tracker Green and DAPI. (B) Alkaline phosphatase (ALP) staining of MSCs after 7 days of EV treatment. (C) Biochemical quantification of ALP activity ($n = 5$). Data are presented as mean ± SD; $^*p < 0.05$ vs. Control-EVs group by one-way ANOVA.

group (Fig. 4D). These results indicated that BMP2-EVs could enhance the osteogenic differentiation of MSCs in hydrogels.

It is generally believed that comprehensive vascularization is essential for obtaining strong regenerative tissues. CD31 is an important factor affecting the vascular network[25]. CD31 may also have other specific functions. It not only stimulates angiogenesis but also indirectly affects the differentiation and maturation of osteoblasts[26]. When grown in BMP2-EVs collagen hydrogels, MSCs showed stronger expression of CD31 and alkaline phosphatase (Fig. 4E).

Alizarin red S staining of calcium salt nodules usually reflects mineralization. After 14 days of osteogenic induction, compared with the Control-EVs group, the BMP2-EVs group showed enhanced alizarin red S staining and quantitative analysis; in contrast, the Noggin-EVs group showed a decrease (Fig. 4F and G). These results indicated that BMP2-EVs enhanced the mineralization of MSCs in collagen hydrogels.

The BMP/SMAD/RUNX2 signaling pathway is well-established as crucial for bone formation[27]. In this study, we investigated the effect of BMP2 delivered by BMP2-EVs on pSMAD1/5/8 activation to elucidate the underlying mechanism. Following a 48-hour incubation of MSCs with EVs under two-dimensional culture conditions, quantification revealed that BMP2-EVs delivered significantly higher levels of BMP2 protein to MSCs compared to Control-EVs and Noggin-EVs (Fig. 4H, I). Concomitantly, BMP2-EVs induced markedly greater formation and nuclear accumulation of phosphorylated SMAD1/5/8 complexes (Figure. 4 J, K). Collectively, these data demonstrate that BMP2-EVs effectively activate the canonical BMP/SMAD signaling pathway.

BMP2-EVs promote the migration of MSCs

Given the crucial role of cell migration in the early stage of bone repair, we further investigated the effect of BMP2-EVs on the migratory behavior of MSCs in vitro. Extracellular vesicles from MSCs can promote the migration of stem cells and osteoprogenitor cells to the defect site, which then form new bone through proliferation and osteogenic differentiation. The migration activity of cells was detected using transwell chamber assays. We found that, compared with Control-EVs, BMP2-EVs had a stronger ability to promote stem cell migration. In contrast, Noggin-EVs reduced this migration-promoting ability (Fig. 5).

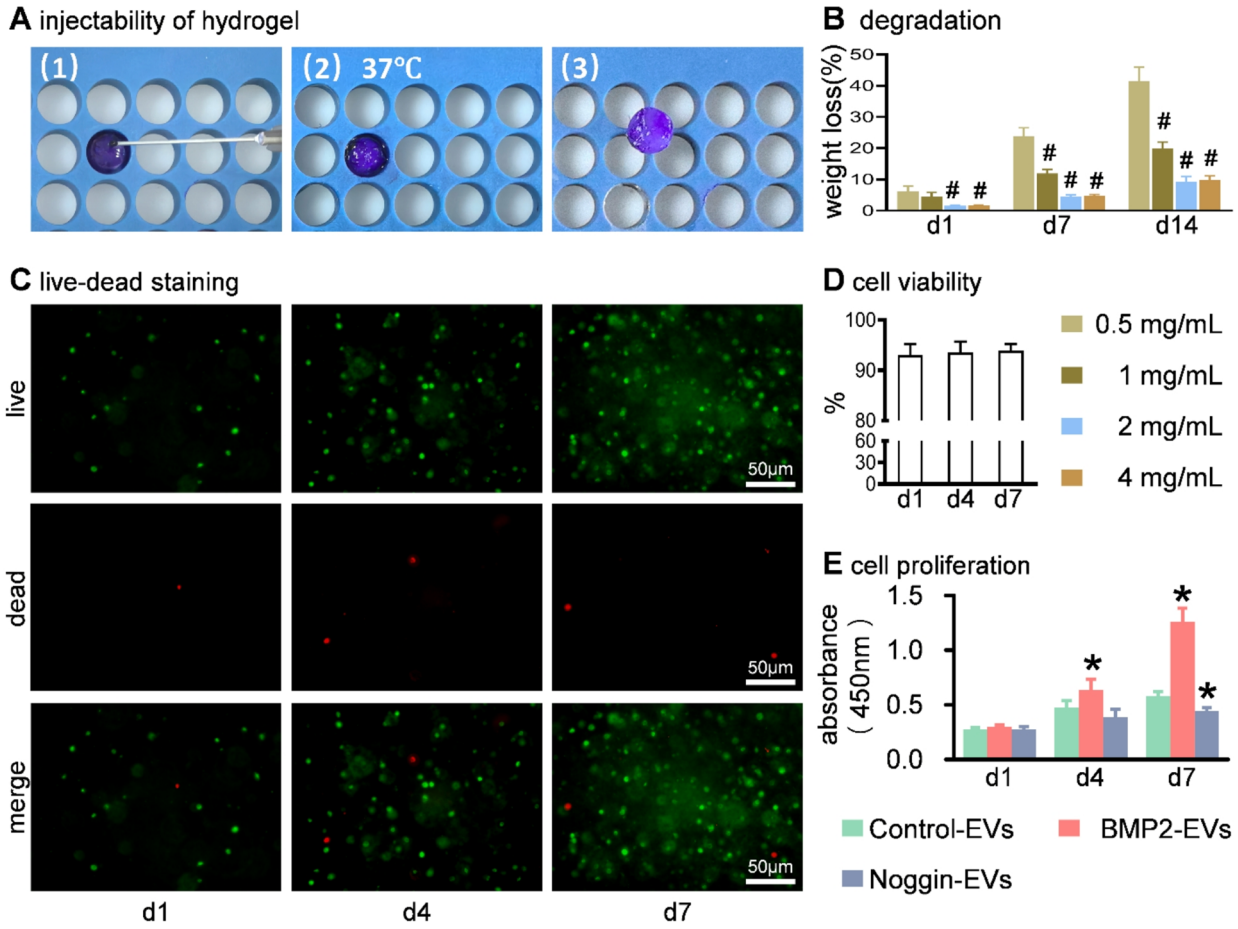

Fig. 3. Preparation and biocompatibility assessment of collagen hydrogel. (A) Injection and thermogelation process of collagen hydrogel. (B) Degradation rate of collagen hydrogels at different concentrations ($n = 5$). #$p < 0.05$ vs. 0.5 mg/mL group by one-way ANOVA. (C, D) Live/dead staining and quantitative analysis of MSCs in the BMP2-EVs group. (E) Cell proliferation assessed by CCK-8 assay ($n = 5$). Data are presented as mean ± SD; *$p < 0.05$ vs. Control group by one-way ANOVA.

BMP2-EVs-loaded hydrogel promotes bone regeneration in vivo

To validate the in vivo efficacy of this injectable system, we applied it to a mouse femoral defect model and evaluated its bone regeneration capacity through radiographic and histological analyses. Given the limitations of natural collagen sponges in directly combining with BMP2 (which often leads to poor treatment outcomes due to their rapid clearance), we adopted extracellular vesicles with good binding ability to collagen as the delivery carrier. This strategy not only reduces the risk of burst release but also takes advantage of the natural tendency of extracellular vesicles towards the bone microenvironment.

Here, we evaluated the BMP2 retention efficiency of cell-free BMP2-EVs-loaded collagen hydrogels in vitro. We measured the amount of BMP2 released into the PBS solution and then calculated the amount of BMP2 retained on the collagen hydrogels over 2 weeks based on the total loading amount. The results showed that BMP2-EVs-loaded collagen hydrogels had a slow-release effect on BMP2. The amounts of BMP2 remaining on the collagen hydrogel at days 1, 4, 7, 10, and 14 were 91%, 82%, 74%, 68%, and 61%, respectively (Fig. 6A).

For in vivo evaluation, temperature-responsive collagen solution loaded with 30 μg/mL BMP2-EVs (with a BMP2 concentration of 319 ng/mL) was injected into 1 mm sized distal femoral defects of mice. The collagen solution self-formed the hydrogel in response to temperature and matched the shape of the defect area (Fig. 6B). Tissues were harvested after 4 weeks of implantation. Micro-CT showed that BMP2-EVs significantly promoted new bone formation (Fig. 6C, D).

Hematoxylin-eosin staining showed that there were significant osteogenic patterns among the different groups. The blank group form clearly visible bone defect cavities, indicating that the model construction was successful. The hydrogel group showed only a very weak osteogenic response. The control-exosome group showed a weak osteogenic response. It is notable that BMP2-EVs induced a strong osteogenic response, manifested as interconnected bone structures throughout the defect center. In contrast, the bone formation in the Noggin-EVs group was significantly reduced, accompanied by large areas of cavities (Fig. 6E, F). Quantitative analysis confirmed these observations: the bone volume fraction (BV/TV), the number of osteoblasts per tissue area (N.Ob/T.Ar), and the number of osteoblasts per bone surface (N.Ob/B.S) in the BMP2-EVs group were

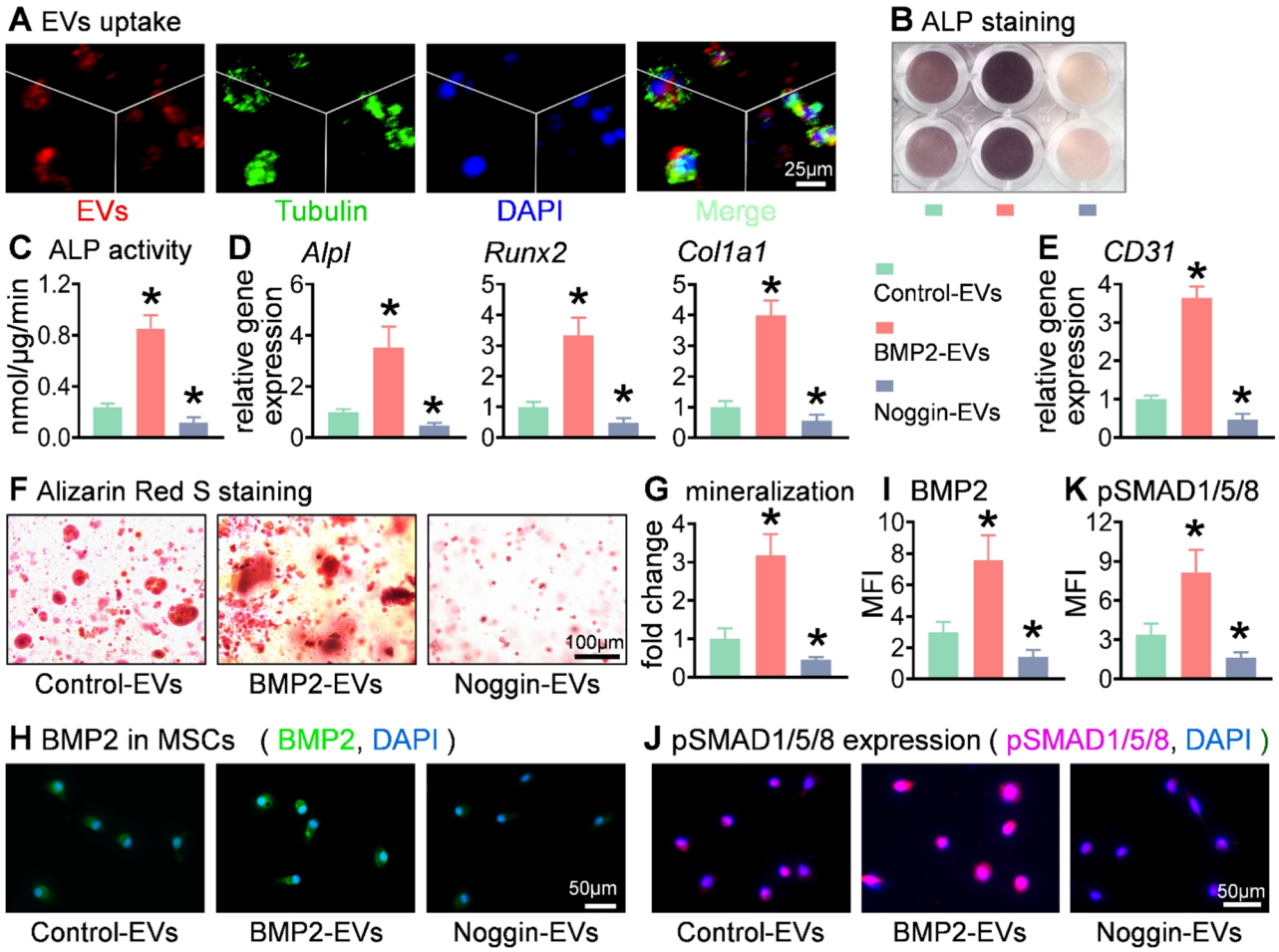

Fig. 4. BMP2-EVs promote osteogenic differentiation of MSCs in collagen hydrogels. (A) Uptake of red fluorescent-labeled BMP2-EVs by MSCs in hydrogel. (B) ALP staining and (C) biochemical quantification of ALP activity. (D) Expression of osteogenic genes. (E) Expression of the angiogenesis factor CD31. (F) Alizarin Red S staining and (G) quantitative analysis of mineralization. (H-K) BMP2 and pSMAD1/5/8 immunofluorescence staining and quantification in MSCs under 2D culture ($n = 5$). MFI, mean fluorescence intensity. Data are presented as mean ± SD; $^*p < 0.05$ vs. Control-EVs group by one-way ANOVA.

significantly higher than those in the Control-EVs group ($p < 0.05$). Conversely, the osteogenic parameters in the Noggin-EVs group were decreased. Overall, these research results indicate that this injectable BMP2-EVs hydrogel system can achieve effective minimally invasive bone repair by controlling the release of BMP2 and enhancing osteogenic activity, thus providing a promising treatment strategy for bone defects.

BMP2-EVs-loaded hydrogel promotes the formation of vascularized bone

Since the coupling of osteogenesis and angiogenesis is critical for high-quality bone regeneration, we finally evaluated the potential of this treatment system to promote vascularized bone formation by detecting specific markers. The osteogenic and angiogenic potential of BMP2-EVs hydrogels was evaluated using multi-analytical approaches. Masson's trichrome staining and Sirius red staining results showed that, compared with the Control-EVs group, the BMP2-EVs-loaded hydrogels had a significant bone increase (Fig. 7A). Corresponding to the enhanced bone formation observed, the expression of RUNX2 and OSTERIX(OSX) in the BMP2-EVs group was also significantly increased (Fig. 7B and C). In contrast, the Noggin-EVs group showed reduced collagen formation. This was consistent with the results of HE observation, where the BMP2-EVs hydrogels induced the strongest osteogenic response of RUNX2 and OSTERIX.

CD31 and Endomucin are key markers of type H angiogenesis, which is related to osteogenesis[28]. Using double-immunofluorescence staining, we found that, compared with the Control-EVs group, the overlapping expression intensity of CD31 and Endomucin in the BMP2-EVs group was enhanced by 2.9-fold. In contrast, both the total amount and the overlapping expression intensity of CD31 and Endomucin in the Noggin-EVs group were decreased (Fig. 7D and E). The above data directly reflected the significant promoting effect of the BMP2-EVs group on angiogenesis-related indicators.

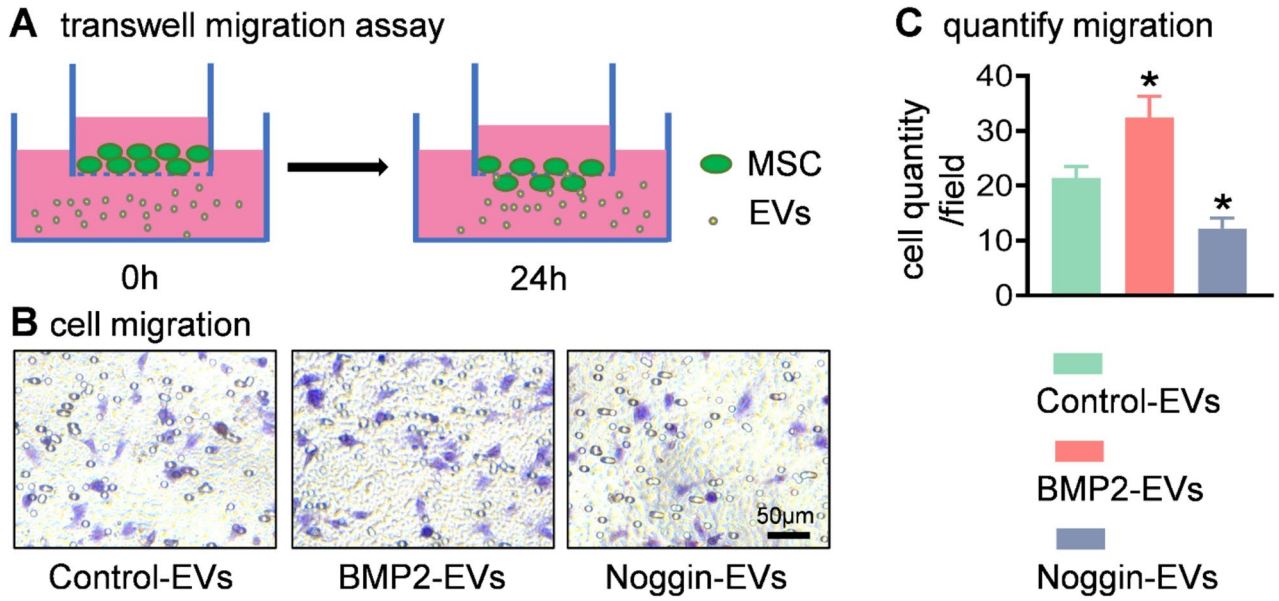

Fig. 5. **BMP2-EVs enhance MSCs migration.** (A) Schematic diagram of the Transwell (8 μm) cell migration assay. (B, C) BMP2-EVs promote MSC migration in the Transwell assay. Representative images of the cells that were migrated to the bottom surface of the Transwell chamber after being stained with crystal violet (the blue spots represent the cells). EVs: Extracellular vesicles. $n = 5$. Data are presented as mean ± SD; $^*p < 0.05$ vs. Control-EVs group by one-way ANOVA.

Discussion

Bone morphogenetic protein 2 (BMP2) is a potent osteogenic factor whose clinical application is limited by its rapid release from absorbable collagen sponges, short in vivo half-life, and requirement for supraphysiological doses, which often lead to adverse effects including ectopic ossification and neuroinflammation[29]. To overcome these challenges, we developed a cell-free therapeutic strategy combining BMP2-loaded mesenchymal stem cell-derived extracellular vesicles (BMP2-EVs) with an injectable, temperature-responsive collagen hydrogel, establishing a synergistic platform for minimally invasive bone regeneration.

Using a recombinant adenovirus-mediated expression system, we enabled MSCs to secrete EVs highly enriched with BMP2. Quantitative analysis revealed that BMP2-EVs contained 3.3 times more BMP2 cargo compared to EVs derived from MSCs. MSC-derived EVs have limited ability to promote the osteogenic differentiation of MSCs[30]. Noggin binds BMP2 and prevents docking of BMP2 to its surface receptor, thereby inhibiting osteogenic differentiation of osteogenic progenitor cells[31]. In this study, BMP2-EVs demonstrated stronger osteoinductive capacity than stem cell EVs, upregulating alkaline phosphatase activity by 2.9-fold ($p < 0.05$). On the contrary, the reduced osteogenesis of EVs produced by MSCs after Noggin induction further validated the specificity of BMP2-EVs-mediated osteogenesis regulation.

The collagen hydrogel component leveraged the inherent bioactivity of type I collagen, which self-assembles at body temperature into a nanofibrous matrix mimicking the native bone extracellular matrix. Such local exosome delivery systems have shown promise in regenerating skin, spinal cord, and bone tissues[32–34]. Our collagen hydrogel demonstrated excellent cytocompatibility, supporting over 92% MSC viability after 7 days in culture. It served dual functions: providing mechanical support for cell infiltration and acting as a reservoir for controlled BMP2-EVs release. Additionally, BMP2-EVs enhanced MSC migration—a critical process for recruiting progenitor cells to injury sites during bone repair[35].

The BMP/SMAD/RUNX2 pathway plays a central role in osteogenesis[27][36]. We confirmed that BMP2 delivered via BMP2-EVs activates SMAD1/5/8 phosphorylation, upregulates the master transcription factor RUNX2 , and enhances expression of early osteogenic markers such as *Alpl* and *Col1a1*. This cascade ultimately drives osteoblastic differentiation of MSCs, with the enhanced efficacy of BMP2-EVs attributable to their improved BMP2 delivery efficiency.

In a mouse femoral defect model, the collagen solution underwent sol-gel transition at body temperature, conforming precisely to the defect site. The BMP2-EVs group exhibited significantly superior bone repair, with 3.2-fold and 3.3-fold increases in bone volume fraction (BV/TV) and osteoblast density (N.Ob/T.Ar), respectively, compared to the Control-EVs group.

Type H vessels, marked by CD31 and Endomucin co-expression, play a pivotal role in coupling angiogenesis and osteogenesis[37]. These vessels serve as regulatory niches, secreting factors that stimulate osteoprogenitor cells—many of which express OSTERIX—to differentiate into osteoblasts[38]. In our study, BMP2-EVs significantly enhanced CD31 and Endomucin expression, with a 2.9-fold increase in their co-localization intensity, consistent with reports that BMP2-induced bone formation is associated with abundant type H vessels[39].

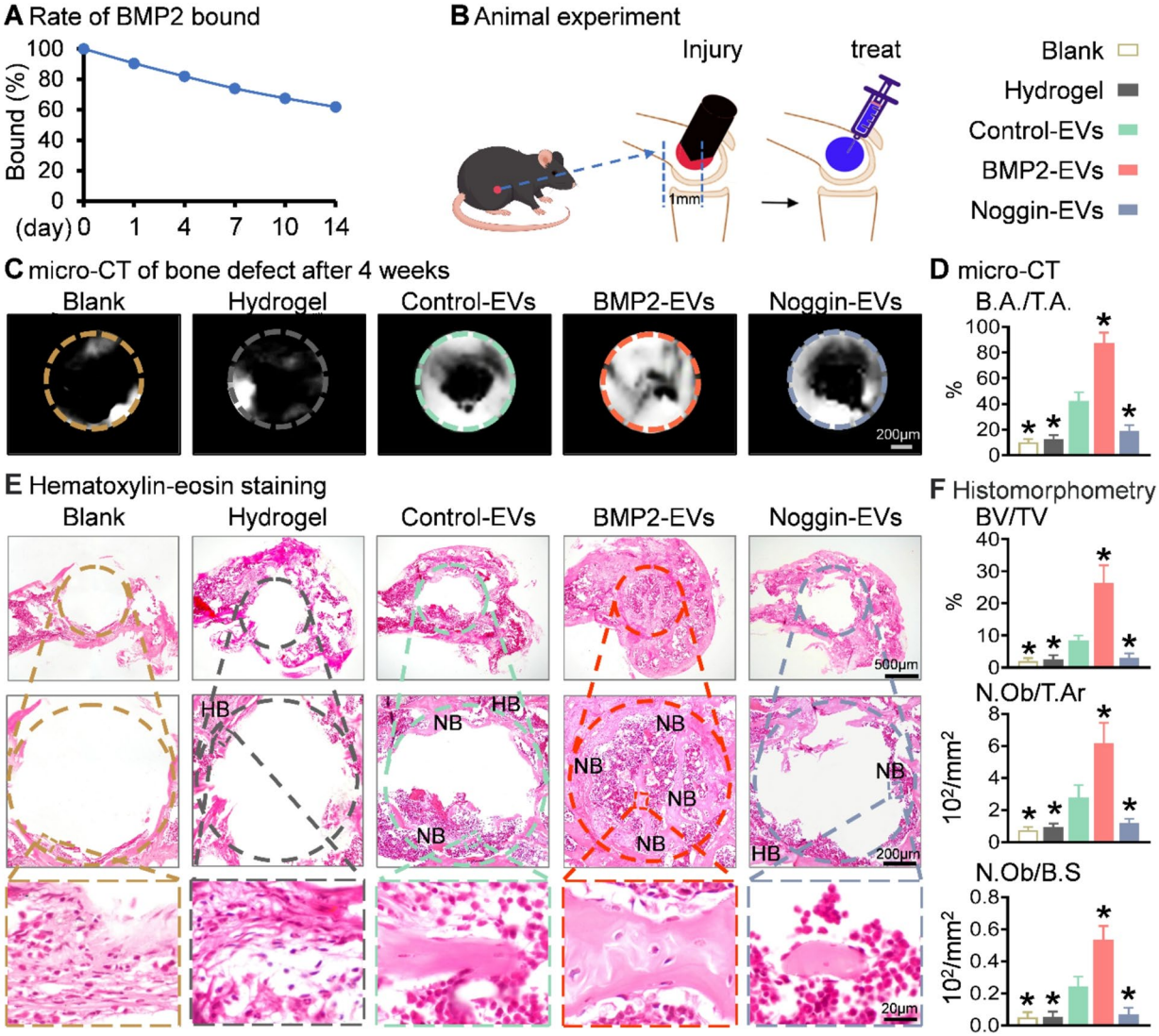

Fig. 6. BMP2-EVs-loaded collagen hydrogel promotes repair of distal femoral bone defects in mice. (A) Retention of BMP2 on collagen hydrogels loaded with BMP2-EVs. (B) Schematic of mouse distal femoral defect creation and in situ injection of collagen hydrogel. (C) Micro-CT images of the defect area at 4 weeks post-surgery (Experimental groups: defect-only, collagen hydrogel, and collagen hydrogels loaded with Control-EVs, BMP2-EVs, or Noggin-EVs) and (D) quantitative analysis of bone area to tissue area ratio (B.Ar/T.Ar). (E) H&E staining. The Control-EVs group showed peripheral new bone formation with central voids, while the BMP2-EVs group exhibited extensive bridging bone formation. HB: host bone; NB: new bone. (F) Bone histomorphometry analysis: BV/TV, N.Ob/T.Ar, and N.Ob/B.S. $n = 5$. Data are presented as mean ± SD; $^*p < 0.05$ vs. Control-EVs group by one-way ANOVA.

Unlike conventional collagen carriers, which release ~ 50% of BMP2 within 2 days, our EV–collagen hybrid system sustained BMP2 release, retaining > 60% of the loaded protein after 14 days. This controlled release enabled effective regeneration at a BMP2 concentration of only 319 ng/mL—far below the clinical dose and lower than the 10,000 ng/mL used in similar studies[8]. This dramatic dose reduction stems from the dual protective role of EVs: surface integrins mediate specific binding to collagen, prolonging retention, while the lipid bilayer shields BMP2 from enzymatic degradation[40]. This provides a safer, more efficient, and cost-effective solution for bone repair therapy.

Although BMP2 delivery is central to this strategy, the enhanced osteogenic potential of BMP2-EVs may not arise solely from BMP2. Overexpression of BMP2 could alter the parental MSC physiology, modifying the RNA (e.g., miRNA, lncRNA) and protein cargo of secreted EVs. miRNA can be involved in the osteogenic function of extracellular vesicles[41]. Future multi-omics analyses will help elucidate contributions from non-BMP2 factors.

Recent studies have combined BMP2 and exosomes for bone regeneration, but our delivery system offers distinct advantages. Unlike GelMA hydrogels that require potentially toxic photo-crosslinkers[23], or multi-injection protocols with poor compliance[42]. our platform uses a chemically crosslinker-free collagen hydrogel that gels in situ, enabling single-injection, sustained release with enhanced safety and convenience.

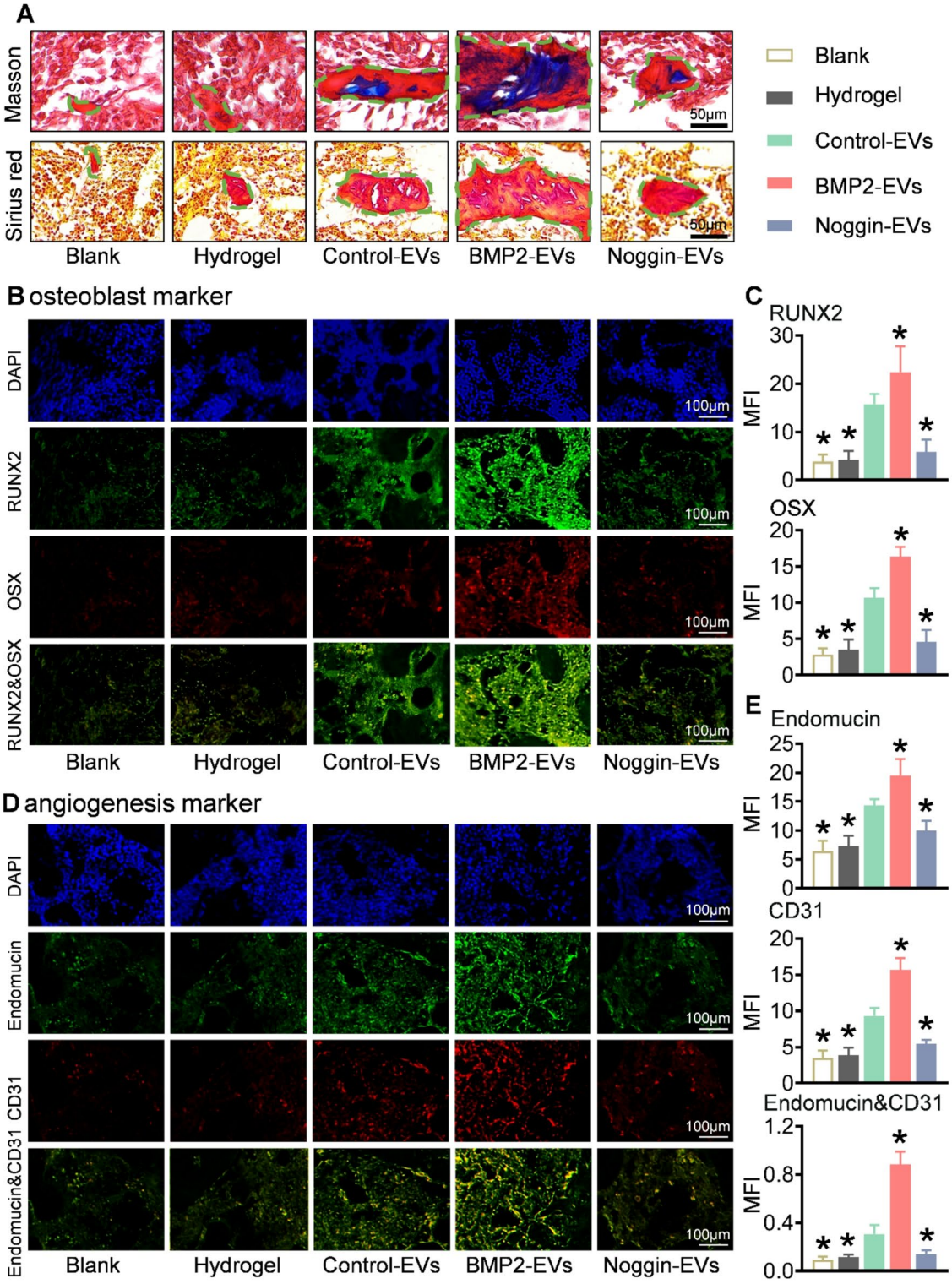

Fig. 7. BMP2-EVs-loaded collagen hydrogel promotes vascularized bone formation. (A) Representative Masson's trichrome staining and Sirius Red staining images of the defect area. The green dashed area indicates the newly formed bone tissue. (B) Representative immunofluorescence images of RUNX2 and OSX(OSTERIX) and (C) quantitative analysis. (D) Representative immunofluorescence staining images of CD31 and Endomucin expression in each group. Yellow fluorescence indicates overlap of CD31 and Endomucin, suggesting the presence of osteogenic type H vessels and (E) quantitative analysis. MFI, mean fluorescence intensity. $n = 6$. $n = 6$. Data are presented as mean ± SD; $^*p < 0.05$ vs. Control-EVs group by one-way ANOVA.

Despite the encouraging results of this study, several limitations remain. Firstly, the sample size in the animal experiments ($n = 6$ per group) is relatively small. Although this sample size is sufficient to detect significant inter-group differences in this study, expanding the sample size is necessary in subsequent large animal model studies to obtain more robust conclusions and assess subtler effects. Secondly, large-scale production of EVs compliant with Good Manufacturing Practice (GMP) standards and cost control represent core bottlenecks. Finally, the long-term biological safety and immunogenicity require more in-depth evaluation. While this study confirmed the short-term safety of the system, further long-term tracking studies over several months to years in larger animal models (such as goats or pigs) are needed to assess the long-term fate, metabolic pathways, and potential immune responses of engineered EVs in vivo.

Conclusion

This study has successfully developed an injectable bone repair system based on BMP2-EVs and a temperature-responsive collagen hydrogel. This system achieves efficient loading and sustained release of BMP2 through genetically engineered EVs, and utilizes a clinically friendly collagen carrier to enable minimally invasive injection and precise in-situ matching of the defect. Experimental results demonstrate that the system can significantly promote the osteogenic differentiation and migration of MSCs, effectively activate the BMP/SMAD signaling pathway, and induce high-quality vascularized bone regeneration in a mouse femoral defect model. Most importantly, the system exhibits superior therapeutic efficacy at extremely low doses of BMP2, providing a novel strategy with tremendous translational potential to overcome the clinical application bottlenecks of BMP2.

Methods

Cell culture

Mouse mesenchymal stem cells (MSCs) were isolated as previously described[43]. Briefly, long bones were harvested from fifteen 2-month-old C57BL/6 mice. Soft tissues were carefully removed, and epiphyses from both ends of the femurs and tibias were excised. Bone marrow cells were flushed out using α-MEM medium supplemented with 1% (v/v) fetal bovine serum (FBS; Gibco, MD, USA). The cells were then seeded in basal medium (α-MEM containing 10% FBS, 100 U/mL penicillin G, and 100 μg/mL streptomycin; Gibco, MD, USA) and cultured at 37 °C with 5% CO_2. After 24 h, non-adherent cells were removed, and adherent cells were collected as MSCs.

Once the MSCs successfully adhered to the surface of the culture vessel, recombinant adenoviruses Ad-BMP2 or its control virus Ad-GFP (kindly provided by the School of Laboratory Medicine, Chongqing Medical University) were added to the culture system. The experimental group was divided into three groups: (1) Control: MSCs transfected with Ad-GFP adenovirus; (2) Ad-BMP2: MSCs transfected with GFP-labeled-Ad-BMP2 adenovirus to overexpress BMP2; (3) Noggin group: MSCs transfected with Ad-GFP adenovirus and treated with 100 ng/mL Noggin (A BMP2 inhibitor, MCE, TX, USA)[44]. Noggin can also reduce CD31 expression and neovascularization[45]. To enhance viral transfection efficiency, 10 μg/mL polybrene (Sigma, MA, USA) was also added in each group. After 24 h of transfection, images were taken using a fluorescence microscopy imaging system (Zeiss, Oberkochen, Germany). After successful transfection, the medium was replaced with a medium containing exosome-depleted fetal calf serum (Cellmax, Beijing, CHINA), and the conditioned medium was collected for exosome isolation.

Isolation and characterization of EVs

Extracellular vesicles were isolated from the conditioned medium according to a previously reported method[46]. Briefly, the conditioned medium was first centrifuged at 300 g for 10 min and then at 2000 g for 10 min to remove cellular components. Next, it was centrifuged at 10,000 g for 40 min to eliminate cell debris and other impurities further. After that, the supernatant was transferred to an ultracentrifuge tube and ultracentrifuged at 100,000 g for 70 min. The supernatant was discarded, and the pellet was retained. The pellet was resuspended in phosphate-buffered saline (PBS) and ultracentrifuged again at 100,000 g for 70 min (using an ultracentrifuge, Thermo Scientific™ Sorvall™ WX100+, T-8100). Finally, EVs were obtained.

The morphology of EVs was observed using transmission electron microscopy (TEM). Concentrated exosome samples from MSCs were fixed with 2.5% glutaraldehyde for 30 min. Then, 10 μl of the mixture was dropped onto a carbon-coated copper grid and air-dried for 10 min. The samples were stained twice with 1% uranyl acetate for 6 min each time. After staining, images of EVs were acquired using an HT7700 transmission electron microscope (Hitachi, Tokyo, Japan) at an accelerating voltage of 120 kV.

The size and concentration of the exosome samples were analyzed in detail using nanoparticle tracking analysis (NTA). The analysis was carried out strictly according to the manufacturer's instructions (ZetaView, Particle Metrix, Germany), and the results were recorded.

Uptake assay of EVs

Extracellular vesicles were labeled with DiI (Thermo Fisher Scientific, MA, USA) to determine their uptake by MSCs. According to the product protocol, EVs diluted in 1 ml of α-MEM were incubated with 5 μl of DiI dye at 37 °C. After 30 min, the labeledEVs were washed in 6 ml of PBS at 100,000 g for 70 min. Then, the DiI-labeled exosome particles were incubated with MSCs for 24 h. After incubation, the cells were washed twice with PBS, and stained with the Tubulin-Tracker Green staining solution (Beyotime Biotechnology, Shanghai, China) for 1 h. The cell nuclei were stained with DAPI solution. Images were captured using a fluorescence microscopy (Nikon, Tokyo, Japan).

Under three-dimensional culture conditions, a collagen suspension containing DiI-labeled extracellular vesicles (EVs) was mixed with MSCs and then injected into cell culture dishes. The mixture was incubated in a cell culture incubator at 37 °C for 30 min to allow the formation of a collagen hydrogel. Subsequently, basal

medium was added for further culture. After 24 h, the uptake of extracellular vesicles by MSCs was observed using a laser scanning confocal microscope (Nikon, Tokyo, Japan).

Screening of the concentration of EVs promoting osteogenic differentiation of MSCs

The protein content of EVs was measured using a BCA protein assay kit (Beyotime Biotechnology, Shanghai, China). To determine the optimal concentration of isolated BMP2-loaded extracellular vesicles for promoting osteogenic differentiation, an experiment was conducted using 24-well plates (Corning, NY, USA). Bone marrow-derived MSCs were seeded into the wells at a density of 8×10^4 cells/well. Different concentrations of EVs (0, 10, 30, and 60 μg/ml) were added to each well. Half of the culture medium was replaced every 3 days. After 7 days of induction culture, alkaline phosphatase staining and alkaline phosphatase activity assays were performed to evaluate the effects of different exosome concentrations on the osteogenic differentiation of the cells.

Preparation and biocompatibility analysis of injectable collagen hydrogels

The concentration of collagen significantly influences the degradation rate of hydrogels. We investigated the in vitro degradation characteristics of collagen hydrogels at varying concentrations. Phosphate-buffered saline (PBS, pH 7.4, 37 °C) effectively simulates the human physiological environment[47,48].

First, Rat Collagen Type I (MERCK, Bavaria, Germany) was dissolved in 0.02 mol/L acetic acid to prepare a 5 mg/mL stock solution. To prepare the hydrogels, every 400 μl of this stock solution was neutralized with 4.6 μl of a 1 mol/L sodium hydroxide (NaOH) solution. The neutralized solution (with a pH of approximately 7.2) was then diluted with pre-chilled sterile water to achieve the target collagen concentrations (0.5, 1, 2, or 4 mg/mL). Next, each diluted solution was added to a 48-well plate, with 500 μl per well. The plate was incubated at 37 °C for 30 min to allow hydrogel formation. After hydrogel formation, the surface liquid on individual hydrogel pieces was wiped dry.

They were then weighed to determine their initial mass. Subsequently, the hydrogels were immersed in PBS at 37 °C. At specified time points (day 1, 7, 14), the samples were removed from the PBS, wiped dry, and weighed again. Finally, the weight loss of the collagen hydrogels at each specific time point was calculated. Building on these results, we used 2 mg/mL collagen, 30 μg/mL EVs, and 1×10^6 cells/mL MSCs in subsequent experiments.

The biocompatibility of the collagen hydrogels was evaluated using cell viability and proliferation assays as reported[49]. A live/dead staining assay was used to assess cell viability in the collagen hydrogels on days 1, 4, and 7. Specifically, 200 μL of LIVE/DEAD viability/cytotoxicity kit (Thermo Fisher Scientific, MA, USA) was added to each well to ensure that the reagent completely covered the cells. The wells were then incubated in an incubator at 37 °C with 5% CO_2 for 60 min. After incubation, the images were detected and captured using a fluorescence microscope. Live cells were stained green, and dead cells were stained red. The ratio of live to dead cells was calculated using ImageJ software. For the cell proliferation assay, a cell counting kit-8 (CCK8) was used to evaluate the cell number according to the manufacturer's instructions (MCE, TX, USA), and a growth curve was plotted based on the absorbance values.

Osteogenic differentiation ability assay

According to a previous method[50], the cell culture plates and collagen hydrogels loaded with cells were stained using a BCIP/NBT alkaline phosphatase color development kit (Beyotime Biotechnology, Shanghai, China). Cell lysates were collected, and alkaline phosphatase activity was measured using an alkaline phosphatase assay kit (Beyotime Biotechnology, Shanghai, China). Specifically, the cells were disrupted using an ultrasonic cell disruptor and then centrifuged at 12,000 × g for 5 min to collect the supernatant. The protein content of the samples was measured using the BCA protein method at a wavelength of 562 nm. Meanwhile, the absorbance was measured using an alkaline phosphatase kit at a wavelength of 405 nm, and the reaction time was recorded. The amount of alkaline phosphatase was calculated based on the standard substrate concentration curve. Finally, the relative alkaline phosphatase activity was calculated according to the protein concentration, alkaline phosphatase concentration, and reaction time.

Mineralization analysis

Matrix mineralization was detected using alizarin red S (Solarbio, Beijing, China) staining, following the method reported[50]. On the 7th day of culture, the hydrogels were placed in an osteogenic induction medium (α-MEM complete medium containing 50 μg/mL ascorbic acid, 5 mM sodium glycerophosphate, and 1 nM dexamethasone) and cultured for an additional 14 days before alizarin red S staining. After staining, the stained matrix was dissolved by incubating with 10% acetic acid for 12 h, and then the solution was neutralized with 10% ammonium hydroxide. The absorbance of the solution was measured at a wavelength of 405 nm to evaluate the degree of matrix mineralization[51].

Cell migration assay

The effect of EVs on MSCs migration was evaluated using a transwell assay. Specifically, 5×10^4 cells were loaded into the upper chamber of a transwell chamber (Corning, NY, USA) with an 8-μm pore filter, and 500 μl of exosome-containing medium was placed in the lower chamber. After 24 h of culture, the chambers were gently washed with PBS. To remove non-migrating cells, the upper part of the membrane was wiped with a cotton swab. Then, the cells were fixed with 4% paraformaldehyde and stained with 0.5% crystal violet (Beyotime Biotechnology, Shanghai, China) for 10 min. The number of migrating cells was counted in five randomly selected microscopic fields per filter to evaluate the effect of EVs on cell migration.

Animal experiments

Thirty male C57BL/6 mice of 8 weeks old were purchased from the Animal Center of Chongqing Medical University. They were randomly divided into five groups, with 6 mice in each group. This study adhered to the ARRIVE principles and the guidelines of the National Institutes of Health (NIH). It was approved by the Institutional Animal Care and Use Committee (IACUC) of the Second Affiliated Hospital of Chongqing Medical University (Approval No: IACUC-SAHCQMU-2024-00066).

Anesthesia was induced with 5% isoflurane and maintained at 1.5%. Following successful anesthesia, the skin was disinfected with povidone-iodine, and an incision was made along the lateral edge of the right femur. The fascia and muscle were sequentially dissected to expose the distal femur. A 1-mm diameter bone defect was created using a drill (MDJ090729, TUUME, China), with intermittent saline irrigation for cooling and removal of bone debris. Subsequently, a 5-μL acellular collagen suspension (30 μg/mL) containing EVs was injected into the defect site using a syringe. The defect-only group and the hydrogel group (without EVs) served as controls. The injected collagen suspension formed a hydrogel in situ at body temperature, conforming precisely to the contour of the defect. Postoperative analgesia was administered via subcutaneous injection of meloxicam (5 mg/kg) for 3 consecutive days. Treatment outcomes were assessed and analyzed by researchers blinded to the group allocation.

Four weeks after the surgery, the mice were euthanized using carbon dioxide asphyxiation. The femoral tissues were first fixed with 4% paraformaldehyde at 4 ℃ for 24 h. The femur was scanned using nanoScan CT (Mediso, Budapest, Hungary) at an energy of 50 kV and an intensity of 165 mas. PMOD software (Zurich, Switzerland) was used to reconstruct the regenerated bone tissue. The region of interest is defined as a dashed circle with a diameter of 1 mm. The ratio of bone area to tissue area (B.A./T.A) was used to evaluate the formation of new bone.

Histopathological analysis

The femur was embedded in paraffin and sectioned to a thickness of 4 μm. The sections were stained with hematoxylin-eosin (H&E, Beyotime, Shanghai, China), Masson's trichrome stain (Solarbio, Beijing, China), and Sirius red stain kit (Solarbio, Beijing, China) to observe the pathological changes in the tissues.

In the immunofluorescence analysis, the sections were subjected to antigen retrieval using EDTA buffer (Solarbio, Beijing, China). Then, the samples were blocked with goat serum and incubated overnight at 4 °C with the following primary antibodies: rabbit anti-RUNX2 monoclonal antibody (Clone No: D1L7F, Abcam, MA, USA), mouse anti-OSTERIX (Clone No: F-3, Santa Cruz, CA, USA), rabbit anti-Endomucin polyclonal antibody (Abcam, MA, USA), and mouse anti-CD31 monoclonal antibody (Clone No: JC/70A, Abcam, MA, USA). After 30 min of incubation with fluorescence-labeled secondary antibodies, images were acquired using a Nikon fluorescence microscope, and the expression of related proteins was analyzed using ImageJ software.

Real-Time quantitative PCR

Total RNA was extracted from the cells using TRIzol reagent (Invitrogen, MA, USA). cDNA synthesis was then performed using a commercial kit from Takara (Tokyo, Japan). Gene expression levels were assessed using real-time quantitative PCR (qRT-PCR). Gapdh was used as an internal control to calculate the relative mRNA expression levels. The forward and reverse primer sequences (5′→3′) for qRT-PCR were synthesized by Sangon Biotech (Shanghai, China) and are as follows: *Bmp2*, GGAAAAGGACATCCGCTCCA and GTGTCTCTTGCA GCTGGACT; *Alpl*, CACGGCGTCCATGAGCAGAAC and CAGGCACAGTGGTCAAGGTTGG; *Runx2*, AAC AGCAGCAGCAGCAG and GCACAGAGCACAGGAAGTTGG; *Col1a1*, GAGCGGAGAGTACTGGATC G and GCTTCTTTTCCTTGGGGTTC; *CD31*, GTCAGAGTCTTCCTTGCCCC and GTCAGAGTCTTCCTT GCCCC; *Gapdh*, GCACAGTCAAGGCCGAGAAT and CCCTTCTCCATGGTGGTGGTGAA.

Western blotting

First, the protein content in the exosome suspension was measured using a BCA protein assay kit (Beyotime Biotechnology, Shanghai, China). The EVs were prepared into samples using RIPA lysis buffer containing protease inhibitors and then separated by eltuectrophoresis on a 10% PAGE gel (Epizyme Biotech, Shanghai, China). The proteins were then transferred to a PVDF membrane.

The membrane was blocked with 5% skim milk in tris-buffered saline and incubated overnight at 4 °C with primary antibodies, including rabbit anti-CD63 polyclonal antibody (Wanleibio, Shenyang, China), rabbit anti-Alix monoclonal antibody (Clone No: E6P9B, CST, MA, USA), rabbit anti-TSG101 polyclonal antibody (Beyotime Biotechnology, Shanghai, China), rabbit anti-BMP2 polyclonal antibody (Beyotime Biotechnology, Shanghai, China), mouse anti-β-ACTIN monoclonal antibody (Clone No: 2D4H5, Proteintech, Wuhan, China), and rabbit anti-GM130 monoclonal antibody (Clone No: D6B1, CST, MA, USA). After washing, the membrane was incubated with horseradish peroxidase-labeled secondary antibodies at room temperature for 1 h. Finally, the membrane was developed using an enhanced chemiluminescence reagent (Invitrogen, California, USA), and the signals were detected and analyzed using the BIO-RAD ChemiDoc MP system.

The original Western blot membranes were cropped to prioritize the presentation of relevant bands and to facilitate multi-target detection under optimal conditions. Uncropped, full-length images of all blots with visible membrane edges are provided in the Supplementary Information File.

Enzyme-Linked immunosorbent assay

To quantify the loading efficiency of BMP2 in EVs, we employed the following procedure: First, the total protein concentration of EVs was determined using a BCA protein assay kit. Subsequently, an equal amount of EVs (based on total protein content) was lysed with RIPA lysis buffer, and the BMP2 content per μg of BMP2-EVs was measured using a BMP2-specific ELISA kit. The method is briefly outlined as follows.

According to the operating instructions of the BMP2 ELISA kit (Lengton, Shanghai, China), the samples were added, followed by the addition of biotin-labeled recognition antigens. The mixture was incubated at 37 °C for 30 min to allow competitive binding with the solid-phase antibodies to form immune complexes. After washing to remove the unbound biotin-labeled antigens, avidin-HRP was added and incubated at 37 °C for 30 min to allow it to bind to the biotin-labeled antigens. After a color-developing reaction, the absorbance was measured at a wavelength of 450 nm, and the BMP2 concentration in the samples was calculated according to the standard curve.By combining this with the previously measured protein concentration of BMP2-EVs, we calculated the BMP2 content per μg of BMP2-EVs.

To evaluate the sustained release of BMP2 from the collagen hydrogel, cell-free collagen hydrogels loaded with BMP2-EVs were incubated in PBS. On days 1, 4, 7, 10, and 14, the PBS was replaced with fresh PBS, and the PBS containing exosomes was collected. The BMP2 content in the collected PBS was then measured using a BMP2 ELISA kit. The amount of BMP2 retained in the gel was determined by subtracting the BMP2 content in the PBS from the total BMP2 amount, and this data was used to plot the BMP2 retention curve.

Cell Immunofluorescence

Following a 48-hour incubation of MSCs with BMP2-EVs, the cells were fixed with 4% paraformaldehyde and subjected to immunofluorescence staining. After blocking with goat serum, the samples were incubated overnight at 4 °C with primary antibodies: rabbit anti-BMP2 polyclonal antibody (Beyotime Biotechnology, Shanghai, China) or rabbit anti-pSMAD1/5/8 polyclonal antibody (Sigma-Aldrich, MO, USA). After washing with PBST, the samples were incubated with fluorescently labeled goat anti-rabbit IgG secondary antibody at room temperature for 30 min. Nuclei were counterstained with DAPI for visualization. Imaging and quantitative analysis were performed using microscopy and ImageJ software, respectively.

Statistical analysis

Statistical analysis was performed using GraphPad Prism 8.0 (GraphPad Prism Software, Inc., San Diego, CA). The experiments involved in this study entailed multiple-group comparisons (≥ 3 groups). Provided that the data conformed to a normal distribution (verified by the Shapiro-Wilk test) and exhibited homogeneity of variances (verified by the Brown-Forsythe test), we conducted an overall significance test using one-way analysis of variance (ANOVA), followed by post-hoc pairwise comparisons using the Bonferroni method. All data are presented as mean ± standard deviation. For data that did not follow a normal distribution, the non-parametric Mann-Whitney U test was applied, and the data are expressed as median and interquartile range. The sample size for the experiments was determined based on our laboratory's prior research and preliminary experimental results, ensuring the ability to detect statistically significant differences given the expected effect size. Statistical significance was defined as $^{*}p < 0.05$.

Data availability

All data generated or analysed during this study are included in this published article.

Received: 27 August 2025; Accepted: 8 December 2025
Published online: 27 December 2025

References

1. Li, Y. et al. Biodegradable magnesium combined with distraction osteogenesis synergistically stimulates bone tissue regeneration via CGRP-FAK-VEGF signaling axis. *Biomaterials* **275**, 120984. https://doi.org/10.1016/j.biomaterials.2021.120984 (2021).
2. Karipidou, N. et al. A critical review of commercial Collagen-Based scaffolds in bone regeneration: functional properties and clinical evidence from Infuse® bone graft. *J. Funct. Biomaterials*. **16**, 313 (2025).
3. Kulikauskas, M. R., Bautch, V. L. & X, S. & The versatility and paradox of BMP signaling in endothelial cell behaviors and blood vessel function. *Cell. Mol. Life Sci.* **79**, 77. https://doi.org/10.1007/s00018-021-04033-z (2022).
4. Bhatti, F. U. R. et al. The effects of high fat diet, bone healing, and BMP-2 treatment on endothelial cell growth and function. *Bone* **146**, 115883. https://doi.org/10.1016/j.bone.2021.115883 (2021).
5. Vantucci, C. E. et al. BMP-2 delivery strategy modulates local bone regeneration and systemic immune responses to complex extremity trauma. *Biomaterials Sci.* **9**, 1668–1682. https://doi.org/10.1039/d0bm01728k (2021).
6. Mumcuoglu, D. et al. Injectable BMP-2 delivery system based on collagen-derived microspheres and alginate induced bone formation in a time- and dose-dependent manner. *Eur. Cell. Mater.* **35**, 242–254. https://doi.org/10.22203/eCM.v035a17 (2018).
7. Wang, H. et al. Phenylboronic acid modified polyethyleneimine alginate Chitosan dynamic hydrogels combination with adipose derived stem cells for controlled delivery of BMP2 to promote bone regeneration and modulating macrophage and angiogenesis. *International J. Biol. Macromolecules*, **329**, 147767 (2025).
8. Han, S. et al. Programmed BMP-2 release from biphasic calcium phosphates for optimal bone regeneration. *Biomaterials* **272**, 120785 (2021).
9. Seims, K. B., Hunt, N. K. & Chow, L. W. Strategies to control or mimic growth factor activity for Bone, Cartilage, and osteochondral tissue engineering. *Bioconjug. Chem.* **32**, 861–878. https://doi.org/10.1021/acs.bioconjchem.1c00090 (2021).
10. Miguez, P. A. et al. Mitigation of BMP-induced inflammation in craniofacial bone regeneration and improvement of bone parameters by dietary hesperidin. *Sci. Rep.* **14**, 2602. https://doi.org/10.1038/s41598-024-52566-7 (2024).
11. Dong, R. et al. Incorporating hydrogel (with low polymeric Content) into 3D-Printed PLGA scaffolds for local and sustained release of BMP2 in repairing large segmental bone defects. *Adv. Healthc. Mater.* **14**, 2403613 (2025).
12. Zhuang, W. et al. A 3D-printed bioactive Polycaprolactone scaffold assembled with core/shell microspheres as a sustained BMP2-releasing system for bone repair. *Biomaterials Adv.* **133**, 112619. https://doi.org/10.1016/j.msec.2021.112619 (2022).
13. Filipović, L., Kojadinović, M. & Popović, M. Exosomes and exosome-mimetics as targeted drug carriers: where we stand and what the future holds? *J. Drug Deliv. Sci. Technol.* **68**, 103057 (2022).
14. Sun, Y. et al. Mesenchymal stem cells-derived exosomes for drug delivery. *Stem Cell Res. Ther.* **12**, 561. https://doi.org/10.1186/s13287-021-02629-7 (2021).
15. Yang, L. et al. Stem cell recruitment polypeptide hydrogel microcarriers with exosome delivery for osteoarthritis treatment. *J. Nanobiotechnol.* **22** https://doi.org/10.1186/s12951-024-02765-1 (2024).

16. Liang, Y. et al. Engineering exosomes for targeted drug delivery. *Theranostics* **11**, 3183–3195. https://doi.org/10.7150/thno.52570 (2021).
17. Cecchin, R. et al. Extracellular vesicles: the next generation in gene therapy delivery. *Mol. Therapy: J. Am. Soc. Gene Therapy*. **31**, 1225–1230. https://doi.org/10.1016/j.ymthe.2023.01.021 (2023).
18. Wang, P. et al. Collagen binding properties separates two functionally distinct subpopulations of milk extracellular vesicles regarding bone regenerative capacity. *Materials Today Bio*, **33**, 102115 (2025).
19. Zeng, M. et al. Emerging trends in the application of extracellular vesicles as novel oral delivery vehicles for therapeutics in inflammatory diseases. *International J. Nanomedicine*, **19**, 8573–8601 (2024).
20. Xi, Y. et al. Injectable thymosin β4-Modified hyaluronic acid hydrogel with exosomes for stem cell homing and Neuronic–Angiogenic–Osteogenic coupled cranial repair. *ACS Nano*. **19**, 22710–22724. https://doi.org/10.1021/acsnano.4c10386 (2025).
21. Chen, L. et al. Multifunctional hydrogel enhances bone regeneration through sustained release of stromal Cell-Derived Factor-1α and exosomes. *Bioactive Mater.* **25**, 460–471. https://doi.org/10.1016/j.bioactmat.2022.07.030 (2023).
22. Bahar, D. et al. Repair of rat calvarial bone defect by using exosomes of umbilical Cord–Derived mesenchymal stromal cells embedded in Chitosan/Hydroxyapatite scaffolds. *International J. Oral & Maxillofacial Implants* **37**, 943-950 (2022).
23. He, Y. et al. BMP2 enhance the osteogenic effect of BMSCs-derived exosomes in skull defect of diabetic rats. *Mater. Design*. **248**, 113517 (2024).
24. Fletes-Vargas, G. et al. Porous Chitosan hydrogels produced by physical crosslinking: physicochemical, structural, and cytotoxic properties. *Polymers* **15**, 2203 (2023).
25. Zhai, Y. et al. Spatiotemporal blood vessel specification at the osteogenesis and angiogenesis interface of biomimetic nanofiber-enabled bone tissue engineering. *Biomaterials* **276**, 121041 (2021).
26. Wang, P. et al. Internal and external co-induction pineal 3D printed scaffolds for bone and blood vessel regeneration. *Mater. Today Adv.* **21**, 100456. https://doi.org/10.1016/j.mtadv.2023.100456 (2024).
27. Zheng, H. et al. Mechanisms and structure-activity relationships of natural polysaccharides as potential anti-osteoporosis agents: A review. *Int. J. Biol. Macromol.* **298**, 139852. https://doi.org/10.1016/j.ijbiomac.2025.139852 (2025).
28. Xu, J. et al. Targeting type H vessels in bone-related diseases. *J. Cell. Mol. Med.* **28**, e18123. https://doi.org/10.1111/jcmm.18123 (2024).
29. Qi, J., Wu, H. & Liu, G. Novel strategies for Spatiotemporal and controlled BMP-2 delivery in bone tissue engineering. *Cell Transplant.* **33**, 09636897241276733. https://doi.org/10.1177/09636897241276733 (2024).
30. Song, Y. et al. Optimizing therapeutic outcomes: preconditioning strategies for MSC-derived extracellular vesicles. *Front. Pharmacol.* **16**, 1509418 (2025).
31. Wu, Z. et al. Regulation of bone homeostasis: signaling pathways and therapeutic targets. *MedComm* 5, e657 (2024).
32. Liu, X. et al. Porous collagen sponge loaded with large efficacy-potentiated exosome-mimicking nanovesicles for diabetic skin wound healing. *ACS Biomaterials Sci. Eng.* **10**, 975–986. https://doi.org/10.1021/acsbiomaterials.3c01282 (2024).
33. Zhang, L. et al. NSCs migration promoted and drug delivered exosomes-collagen scaffold via a bio-specific peptide for one-step spinal cord injury repair. *Adv. Healthc. Mater.* **10**, 2001896. https://doi.org/10.1002/adhm.202001896 (2021).
34. Liu, X. et al. Exosome-loaded hydrogels for craniofacial bone tissue regeneration. *Biomed. Mater.* **19**, 052002. https://doi.org/10.1088/1748-605X/ad525c (2024).
35. Mei, H. et al. Enhanced PDGFR/Wnt/β-catenin activity of mesenchymal stem cells with high migration ability rescue bone loss of osteoporosis. *Cell. Signal.* **97**, 110394. https://doi.org/10.1016/j.cellsig.2022.110394 (2022).
36. Zhu, L. et al. Application of BMP in bone tissue engineering. *Front. Bioeng. Biotechnol.* **10**, 810880. https://doi.org/10.3389/fbioe.2022.810880 (2022).
37. Peng, Y. et al. Type H blood vessels in bone modeling and remodeling. *Theranostics* **10**, 426. https://doi.org/10.7150/thno.34126 (2020).
38. Gao, X. et al. An electrostatic encapsulation strategy to motivate 3D-printed polyelectrolyte scaffolds for repair of osteoporotic bone defects. *Bioactive Mater.* **46**, 1–20. https://doi.org/10.1016/j.bioactmat.2024.12.007 (2025).
39. Yao, H. et al. Controlled release of bone morphogenetic Protein-2 augments the coupling of angiogenesis and osteogenesis for accelerating mandibular defect repair. *Pharmaceutics* **14**, 2397. https://doi.org/10.3390/pharmaceutics14112397 (2022).
40. Wang, J. et al. Surface components and biological interactions of extracellular vesicles. *ACS Nano*. **19**, 8433–8461 (2025).
41. Xu, C. et al. Hydrogel-integrated exosome mimetics derived from osteogenically induced mesenchymal stem cells in spheroid culture enhance bone regeneration. *Biomaterials* **317**, 123088. https://doi.org/10.1016/j.biomaterials.2025.123088 (2025).
42. Li, F. et al. Engineering stem cells to produce exosomes with enhanced bone regeneration effects: an alternative strategy for gene therapy. *J. Nanobiotechnol.* **20**, 135. https://doi.org/10.1186/s12951-022-01347-3 (2022).
43. Siddiqui, I. F. S., Muthu, M. L. & Reinhardt, D. P. Isolation and adipogenic differentiation of murine mesenchymal stem cells harvested from macrophage-depleted bone marrow and adipose tissue. *Adipocyte* **13**, 2350751 (2024).
44. Zhang, M. H. et al. Noggin Combined With Human Dental Pulp Stem Cells to Promote Skeletal Muscle Regeneration. *Stem cells international* 2812390 (2024). (2024).
45. Xu, J. et al. Targeting type H vessels in bone-related diseases. *J. Cell. Mol. Med.* **28**, e18123 (2024).
46. Chen, Y. et al. Protocol for isolating and characterizing extracellular vesicles by ultracentrifugation from bone marrow-derived macrophages. *STAR. Protocols*. **6**, 104098 (2025).
47. Chahsetareh, H. et al. Alginate hydrogel-PCL/gelatin nanofibers composite scaffold containing mesenchymal stem cells-derived exosomes sustain release for regeneration of tympanic membrane perforation. *Int. J. Biol. Macromol.* **262**, 130141. https://doi.org/10.1016/j.ijbiomac.2024.130141 (2024).
48. Kong, B. et al. Structural color medical patch with surface Dual-Properties of wet bioadhesion and Slipperiness. *Advanced science (Weinheim. Baden-Wurttemberg Germany)*. **9**, e2203096. https://doi.org/10.1002/advs.202203096 (2022).
49. Zhu, W. et al. Injectable and assembled calcium Sulfate/Magnesium silicate 3D scaffold promotes bone repair by in situ osteoinduction. *Bioengineering* **12**, 599 (2025).
50. Liu, C. et al. ZFP36 regulates the osteogenic differentiation of adipose-derived mesenchymal stem cells in osteoporosis by mediating KLF3 mRNA degradation. *Sci. Rep.* **15**, 14386. https://doi.org/10.1038/s41598-025-98738-x (2025).
51. Ceylan, S. et al. Molecular Weight-Dependent Boron release effect in PVA/Chitosan cryogels and in vitro mineralization evaluations by osteoblast cells. *Biopolymers* **116**, e23654 (2025).

Acknowledgements

We sincerely thank Chongqing Medical University and the central laboratory of the Second Affiliated Hospital of Chongqing Medical University for their technical and analytical support.

Author contributions

Investigation, G.L. and Z.X.; writing—original draft, G.L.; formal analysis, G.L. and X.F.; conceptualization, G.L. and M.W.; writing—review and editing, M.W. All authors have read and agreed to the published version of the manuscript.

Funding
Thanks to the following projects for their funding support of this study: General Project of Chongqing Natural Science Foundation (CSTB2022NSCQ-MSX0141), General Grant of China Postdoctoral Science Foundation (2023MD744157), Chongqing Postdoctoral Science Foundation (CSTB2023NSCQ-BHX0095), and Chongqing Postdoctoral Special Funding (2023CQBSHTB3040).

Declarations

Competing interests
The authors declare no competing interests.

Author contributions statement
Investigation, G.L. and Z.X.; writing—original draft, G.L.; formal analysis, G.L. and X.F.; conceptualization, G.L. and M.W.; writing—review and editing, M.W. All authors have read and agreed to the published version of the manuscript.

Additional information
Supplementary Information The online version contains supplementary material available at https://doi.org/10.1038/s41598-025-32018-6.

Correspondence and requests for materials should be addressed to M.W.

Reprints and permissions information is available at www.nature.com/reprints.

Publisher's note Springer Nature remains neutral with regard to jurisdictional claims in published maps and institutional affiliations.